Appl. Phys. A (2016) 122:1060
DOI 10.1007/s00339-016-0594-6

Applied Physics A
Materials Science & Processing

Photoacoustic monitoring of water transport process in calcareous stone coated with biopolymers

J. May-Crespo[1] · B. O. Ortega-Morales[2] · J. C. Camacho-Chab[2] · P. Quintana[3] · J. J. Alvarado-Gil[3] · G. Gonzalez-García[4] · M. Reyes-Estebanez[2] · M. J. Chan-Bacab[2]

Received: 19 July 2016 / Accepted: 22 November 2016 / Published online: 30 November 2016

Abstract Moisture is a critical control of chemical and physical processes leading to stone deterioration. These processes can be enhanced by microbial biofilms and associated exopolymers (EPS). There is limited current understanding of the water transport process across rocks covered by EPS. In the present work, we employed the photoacoustic technique to study the influence of three biopolymers (xanthan, microbactan and arabic gum) in the water transport process of two types of limestone rock of similar mineralogy but contrasting porosity. Both controls of RL (low porosity) and RP (high porosity) presented the higher values of water diffusion coefficient (D) than biopolymer-coated samples, indicating that biopolymer layers slowed down the transport of water. This trend was steeper for RP samples as water was transported seven times faster than in the more porous rock. Important differences of D values were observed among samples coated by different biopolymers. Scanning electron microscopy and optical microscopy showed that surface topography was different between both types of rocks; adherence of coatings was seen predominantly in the less porous rocks samples. FTIR and NMR analysis showed the presence of pyruvate and acetate in microbactan and xanthan gum, suggesting their participation on adherence to the calcareous surfaces, sealing surface pores. These results indicate that water transport at rock interfaces is dependent on the chemistry of biopolymer and surface porosity. The implications for reduced water transport in stone conservation under the influence of biopolymers include both enhanced and lower deterioration rates along with altered efficiency of biocide treatment of epilithic biofilms.

1 Introduction

The interest in deterioration processes affecting archeological stone monuments has increased in the past few years. This is partly due to the recognition that a growing number of studies suggest that global climate change will impact built cultural heritage [1]. Global environmental change will have both direct impacts on built heritage; it will also have important indirect effects through its influence on microbial life on heritage sites [2]. Archeological sites in tropical warm and wet climates such as those where Mayan monuments are located are predicted to be affected by altered precipitation, changing the moisture regimes within structures. This understanding is crucial as moisture provides a key control on decay processes [2]. Water can promote dissolution of carbonates and hydrolysis of silicates and is essential for microbial metabolism. Thus, limestone that was used for construction of most Maya buildings is particularly prone to

✉ J. May-Crespo
jose.may@cidesi.edu.mx

✉ B. O. Ortega-Morales
beortega@uacam.mx

[1] CONACYT Research Fellow-Center for Engineering and Industrial Development (CIDESI), Av. Playa Pie de la Cuesta 702. Desarrollo San Pablo, C.P. 76130 Querétaro, Querétaro, Mexico

[2] Departamento de Microbiología Ambiental y Biotecnología, Universidad Autónoma de Campeche, Av. Agustín Melgar s/n, Col. Buenavista, C.P. 24030 Campeche, Campeche, Mexico

[3] Departamento de Física Aplicada, Cinvestav-Unidad Mérida, Carretera Antigua a Progreso, Km. 6, C.P. 97310 Mérida, Yucatan, Mexico

[4] Departamento de Química, División de Ciencias Naturales y Exactas, Campus Guanajuato, Universidad de Guanajuato, Noria Alta S/N, C.P. 36050 Guanajuato, Guanajuato, Mexico

deterioration by chemical dissolution due to its high porosity and mechanically weakness and is also highly bioreceptive by microbial colonizers, causing both important esthetic changes and physical–chemical deterioration [3, 4]. Exacerbated microbial processes associated with cyclic changes in temperature and humidity in tropics make this situation worse.

Microbial communities attached to rock surfaces occur as biofilms; in these biological entities, cells are found embedded in a matrix of extracellular polymeric substances termed EPS [5]. EPS can mediate important processes relevant to the built environment including mineral dissolution, metal solution complexation, biosorption and biomineralization along with particle trapping [4, 6, 7]. This polymeric biogenic matrix is a complex system composed principally of polysaccharides, proteins, lipids, nucleic acids, uronic acids and humic substances, although inorganic material such as carbonates may also occur [5, 8]. The composition and structure of EPS are directly associated with environmental conditions, nutrients and the constitutive microorganisms of biofilm [9, 10]. EPS can have both charged positive or negative moieties and may be involved in biomineralization, leading to a reinforced stone structure [11]. Nevertheless, EPS are often also highly hygroscopic, capturing significant amounts of water [5, 10]. It is reasonable to expect that higher quantities of water or longer times of residence as a consequence of the presence of EPS within stone may contribute to its deterioration [12].

It is crucial to understand moist content of building stones. There are different methods, some can be applied to real-life conditions (walls and monuments), such as electrical resistivity tomography (ERT) technique [13] and infrared thermography [14], while others are mostly used at the laboratory scale and include nuclear magnetic resonance (NMR) [15] and photoacoustic spectroscopy [16].

It has been reported that it is possible to analyze the water permeability using the photoacoustic technique. The main advantage of the photoacoustic technique is that it allows monitoring directly the water transport through the evolution of the thermal contact between the sample and a substrate. Changing the modulation frequency of the modulated light source, which impinges on the substrate, allows controlling the penetration depth of the thermal wave into the rock, optimizing the experimental conditions for the detection of the phenomena. In this sense, thermal wave-based techniques offer superior performance because they offer the possibility of performing thermal depth profiles.

The diffusion coefficients D are obtained from the fitted amplitude normalized signal applying an mass transfer model; therefore, the transport of water inside materials is directly associated with the effective surface porosity [16]. The water diffusion coefficient D (with units m^2/s) is the proportionality constant relating the flux due to molecular transport and the gradient in water concentration. Higher values of this coefficient indicate that the water will move faster into the sample.

In principle, this technique is not foreseen as tool to be used under field (real-life) conditions, but a technique valuable to study factors influencing water transport in rocks and also to screen materials suitable for stone consolidation. In the current study, photoacoustic spectroscopy has been applied to determine the influence of polymeric films in water transport processes deposited onto the surface of limestone rocks. Three natural polymers were evaluated, including an exopolymer from *Microbacterium* sp. named microbactan [17] and two commercial polymers (xanthan and arabic gums of bacterial and plant origin, respectively).

It is hypothesized that the presence of biopolymers on the surfaces of rocks diminishes the water diffusion coefficient, slowing down the transport of water across the rock sample. We expected that this velocity is dependent on the chemical composition of biopolymers and on the surface porosity of the substratum. Moreover, it can be expected that microbial polymers (xanthan gum and microbactan) that possess anionic functional groups have a different behavior than neutral polysaccharides.

2 Experiments

2.1 Rock samples

Two different limestone rock samples, named RL (low porosity) and RP (high porosity), were collected from different quarries from the state of Yucatán, México. The determination of physical properties such as dry density, water absorption and water content was carried out according to ASTM standard D2216-98 [18], and its effective porosity percentage was determined using the saturation technique [19]. The rock samples were cut using a precision saw (Buehler Isomet) with a diamond tip disk (Buehler). Afterward, it was polished with sandpaper, beginning with a large grain size of 220 and ending with fine grain of 2000. Then, the samples were cleaned with ethanol for 2 min with an ultrasonic bath and finally were dried in a furnace at 110 °C for 4 h. A total of 24 cylinders were analyzed, with a final thickness of 1 mm and a diameter of 6 mm.

X-ray diffraction was used for the identification of the studied materials. Structural characterization of limestone samples was carried out by XRD in a Siemens (D-5000) diffractometer operated at 34 kV and 25 mA, with CuKα radiation ($\lambda = 1.5418$ Å) and registered within 3°–45° 2θ range, with a time step of 6 s and a step size of 0.02°. Calcium carbonate was dissolved with HCl solution 5% (v/

v), in order to see the presence of minor minerals, and then identified by XRD. Scanning electron microscopy and optical microscopy were used to analyze the surface of the rocks and the effect of the presence of polymer coatings. The surface morphology of rock samples was observed after the polymeric coating application using environmental scanning electron microscopy (SEM), Philips model XL30 and an optical microscope (MO), Labtronic Scientific (DIN-125).

2.2 Biopolymers

Microbactan was produced following a batch shake flask fermentation of an overnight culture (50 mL) of *Microbacterium* sp. MC3B-10 as previously reported [20]. The exopolymeric material was extracted from the fermented broth, redissolved in a small volume of distilled water and then dialyzed (molecular weight cutoff 12,000–14,000 Da, Spectrum®, CA, USA) for 72 h. The resulting material was lyophilized and characterized. According to Ref. [20], microbactan is a non-toxic EPS of glycolipoproteic nature of high molecular weight (700 kDa). Xanthan gum is a commercial bacterial polysaccharide (ICN Biomedicals, Inc., Irvine, CA, USA), and arabic gum is a commercial plant-derived polysaccharide (Spectrum®). The purpose of NMR analysis was to determine the eventual presence of anionic substituents such as pyruvate and acetate known to be calcium-binding sites. Each biopolymer was dissolved in 600 μL of D_2O. ^1H (599.8 MHz) NMR spectra were recorded at 25 or 45 °C on a Varian/Agilent Premium Compact 600 NMR spectrometer with π/4 pulse of 4.3 μs, 1.0 s of inter-pulse delay, 128 number of scans and 5.0 s of acquisition time. Chemical shifts (ppm) were determined relative to internal 3-(trimethylsilyl) propionic-2,2,3,3-d_4 acid, sodium salt (TMSP-d_4) at 0.0 ppm.

IR spectra in the transmittance mode of biopolymers were recorded on a Thermo Nicolet Nexus 670 spectrometer equipped with a DTGS KBr detector in the middle infrared band (4000–400 cm^{-1}). The samples (5 mg) were mixed thoroughly using an agate mortar with potassium bromide (95 mg) until homogenization. The mixture was inserted into the sample compartment at the Smart Multi-Bounce HATR of the spectrometer and continuously purged with dry air. The number of scans for each spectrum was 64, and the spectral resolution was 4 cm^{-1}. This analysis was done to confirm the chemical nature of the tested polymers.

2.3 Coating of rock samples

The rock samples were coated with a polymeric solution of 1% (w/v) of each polymer. The coated surfaces were allowed to dry under laboratory conditions; this treatment was applied by capillary absorption for 10 min; then, the samples were maintained horizontally at room temperature for 5 days.

2.4 Measurement of water transport by photoacoustic technique

PA technique was used due to its simplicity, high sensitivity and stability to perform studies of time-dependent process such as mass diffusion. The influence of polymeric films in the water permeation process was analyzed by the PA technique. The study was performed using a modified Rosencwaig PA cell, in which the sample is illuminated with a modulated red laser beam at a fixed frequency [21]. It consisted of a conventional PA cell, closed on one side by a transparent window and on the other by aluminum foil of 25 μm thickness (Fig. 1). In the experimental configuration, the aluminum substrate is illuminated by the 658 nm laser light. Main light absorbers are the electrons of the foil; therefore, 658 nm light penetrates only in a very thin layer of the aluminum depending on the roughness and inducing a strong reflection of the light [22]. On the top of this foil, each sample was attached using thermal paste. The sample was illuminated through the quartz transparent window. An electret microphone is used, coupled to the cavity wall, to register the pressure fluctuations in the PA chamber produced by the periodic heating of the aluminum, due to the pumping beam of a 160-mW diode laser at 658 nm (ML120G21) modulated at a constant frequency of 7 Hz. The microphone signal is fed into a lock-in amplifier (SR830), from where the output signal amplitude is recorded, as a function of time. In order to obtain results independent of the specific characteristics of the microphone, the PA signal at any time was normalized with respect to the PA signal before the water drop was deposited.

For the configuration used in the work (Fig. 1), and taking into account that under the conditions used the thermal diffusion length is much shorter than the width of the sample [16], the PA signal is given by:

$$\theta = \frac{I_0}{2\sqrt{\pi f}(1+i)\sqrt{k\rho C}} \quad (1)$$

where k, ρ and C are the thermal conductivity, density and specific heat of the sample, f and I_0 are the modulation frequency and intensity of the laser beam. The factor $\sqrt{k\rho C}$ can be written as a function of the initial conditions (before the start of the mass diffusion process) as well as the thermal conductivity, density and heat capacity of the water and rock matrix as well as the concentration of water in the rock. On the other hand, solving the time-dependent mass diffusion equation for the water entering the rock, it

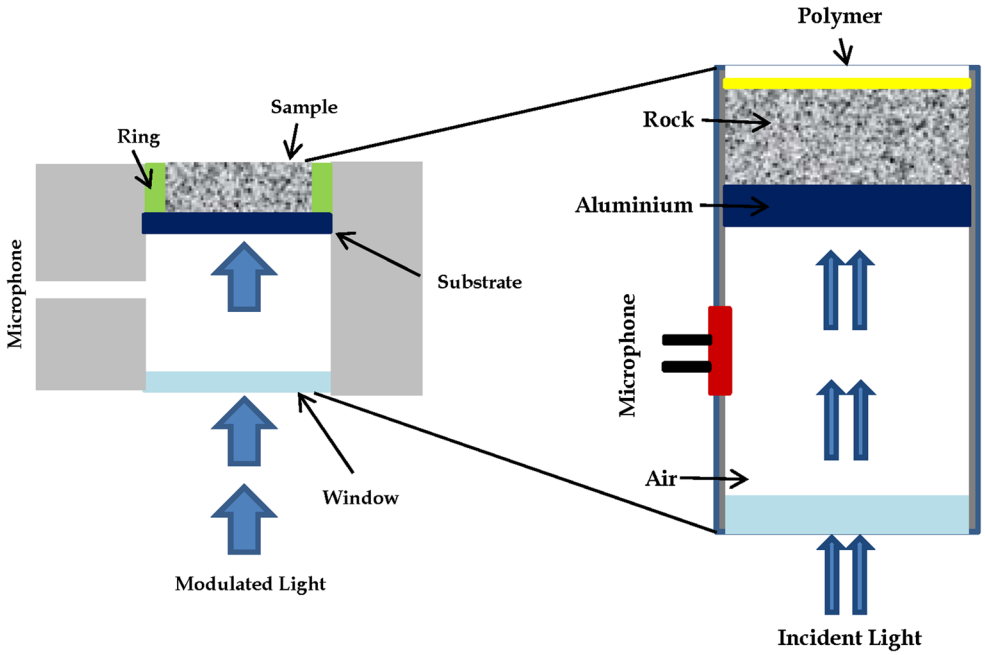

Fig. 1 Schematic cross section of the conventional photoacoustic cell

can be shown that the mass of the water entering the rock depends on the water diffusion coefficient, the final mass of water and the thickness of the sample. Combining these theoretical results, the water diffusion coefficient can be determined by fitting the experimental data. The errors for the diffusion coefficient were determined taking into account the uncertainties involved in the thickness, mass measurements as well as on the fittings.

3 Results

3.1 Characterization of rocks

XRD analysis indicates that calcite ($CaCO_3$) was the predominant crystalline phase; traces of quartz (SiO_2) were also detected. Due to the high percentage of calcite (around 90%), the carbonates were dissolved in order to analyze the remaining mineral traces, others than SiO_2. XRD patterns of the powders after dissolution of the carbonates indicate that for RL (low porosity) and RP (high porosity) the content of the crystalline mineral phases is similar, showing the presence of anatase (TiO_2) and clays such as tosudite $[(KCa)O_8Al_6(SiAl)_8O_{20}(OH)_{10}4H_2O]$, smectite $[Ca_{0.2}(Al,Mg)_2Si_4O_{10}(OH)_2 4H_2O]$ and kaolinite ($Al_2Si_2O_5(OH)_4$). The microscopic observations (Fig. 2) revealed that RP is made predominantly of calcified microorganisms and marine shell fragments. SEM images (Fig. 2c, d) showed that the RL limestone had a pore size smaller than 10 μm, in contrast to RP which exhibited zones of higher levels of porosity and also a widespread heterogeneous distribution. The physical properties of the two types of rock (lithotypes) are listed in Table 1. These data showed that the dry density value was higher for RL than for RP, although the percentage of water absorption, water content and effective porosity for RP were around five times higher in comparison with RL. These data in general revealed that from the chemical point of view both lithotypes were similar, but contrasting in their physical properties, in particular those related to their behavior toward water storage and holding.

3.2 Characterization of biopolymers by FTIR and NMR

The FTIR spectra of the biopolymers showed a broadband around 3420 cm^{-1} characteristic of OH and NH groups and a weak CH_3 stretching band at 2920 cm^{-1} (Fig. 3a–c). The peak around 2140 cm^{-1} corresponds to aliphatic C–H compounds. The observed band at 1720 cm^{-1} was related to C=O stretching of amides. In the middle wavenumber range, the peak at 1540 cm^{-1} was associated with NH amide bending and CH stretching vibrations. In the range from 1200 to 990 cm^{-1}, the bands were associated with CH_2 groups from acids and esters. The peak at 1160 cm^{-1} is due to the presence of glucuronic acid, mannuronic acid and *o*-acetyl ester [23]. The microbactan spectrum can be observed as a weak symmetrical stretching peak near 1410–1330 cm^{-1}, due to the presence of carboxyl groups, which can also be detected in xanthan that showed an

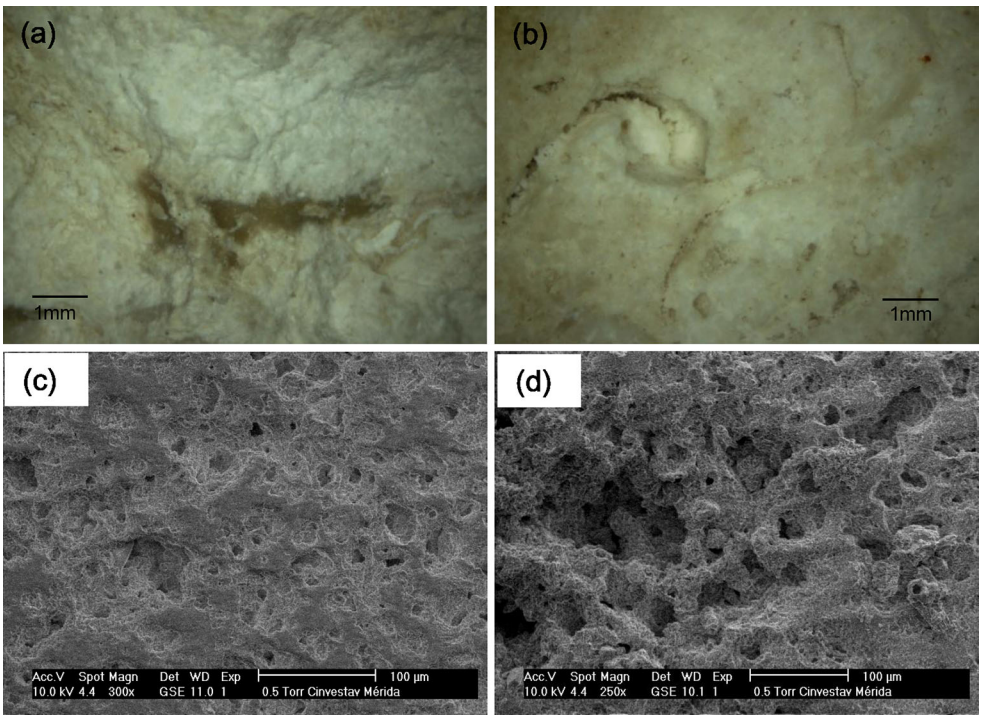

Fig. 2 Optical microscope images: **a** RL surface, **b** RP surface coupon and SEM images: **c** RL shows a pore size less than 10 µm, **d** RP presents a heterogeneous distribution and high porosity for natural samples

Table 1 Physical properties displayed by two different lithotypes

	RL (low porosity)	RP (high porosity)
Dry density (g/cm^3)	2.23 ± 0.06	1.48 ± 0.03
Water absorption (%)	3.63 ± 0.07	18.08 ± 2.37
Water content (%)	0.27 ± 0.03	1.50 ± 0.04
Effective porosity (%)	6.58 ± 0.65	34.40 ± 1.79

additional peak at 1720 cm^{-1}. The band around 980 cm^{-1} was due to CH_2 from the saccharide rings, which only appeared for xanthan and microbactan biopolymers. These data confirmed the chemistry of the three polymers.

Figure 4a shows the ^{1}H NMR spectrum of microbactan at 25 °C; peaks at 5.35 and 5.07 ppm were assigned to the α-anomeric protons of hexose and the peak at 4.60 ppm corresponds to the β protons of hexose. The pyruvate and acetate groups were identified at 1.34 and 2.04 ppm, respectively. Xanthan gum is a β-(1,4)-linked repeating heteropolymer consisting of pentasaccharide units of glucose, mannose and glucuronate. Figure 4b shows the ^{1}H NMR spectrum of commercial xanthan at 45 °C; although this spectrum is quite complex, it was possible to identify peaks that are attributed to the α-anomeric protons of hexose (5.37, 5.18, and 4.96 ppm) and also pyruvate (1.47 and 1.32 ppm) and acetate (2.16 ppm) groups. NMR data of both microbactan and xanthan gum possess anionic behavior given the presence of acetate and pyruvate groupings. ^{1}H NMR spectrum

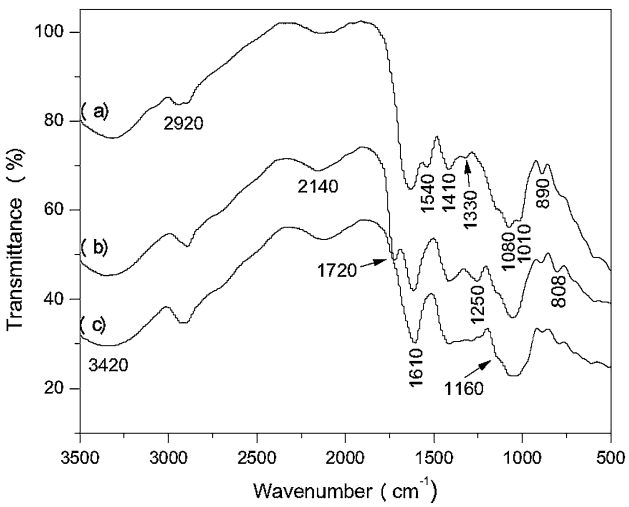

Fig. 3 FTIR spectra for the biopolymers: *a* microbactan, a stretching peak at 1410–1330 cm^{-1}, indicates the presence of carboxylic groups, *b* xanthan gum, band around 980 cm^{-1} was due to CH_2 from saccharide rings and *c* arabic gum, band at 1160 cm^{-1}, corresponds to glucuronic acid

of arabic gum at 25 °C shows peaks at 5.41, 5.31, 5.27, 5.04 and 4.51 ppm, which are assigned to the anomeric protons, and the peak at 1.27 ppm can be assigned to the methyl group of rhamnose units (Fig. 4c).

SEM images of the stone surface after the application of the polymeric films are shown in Fig. 5. It is clearly observed that the coatings on the surface for RP and RL

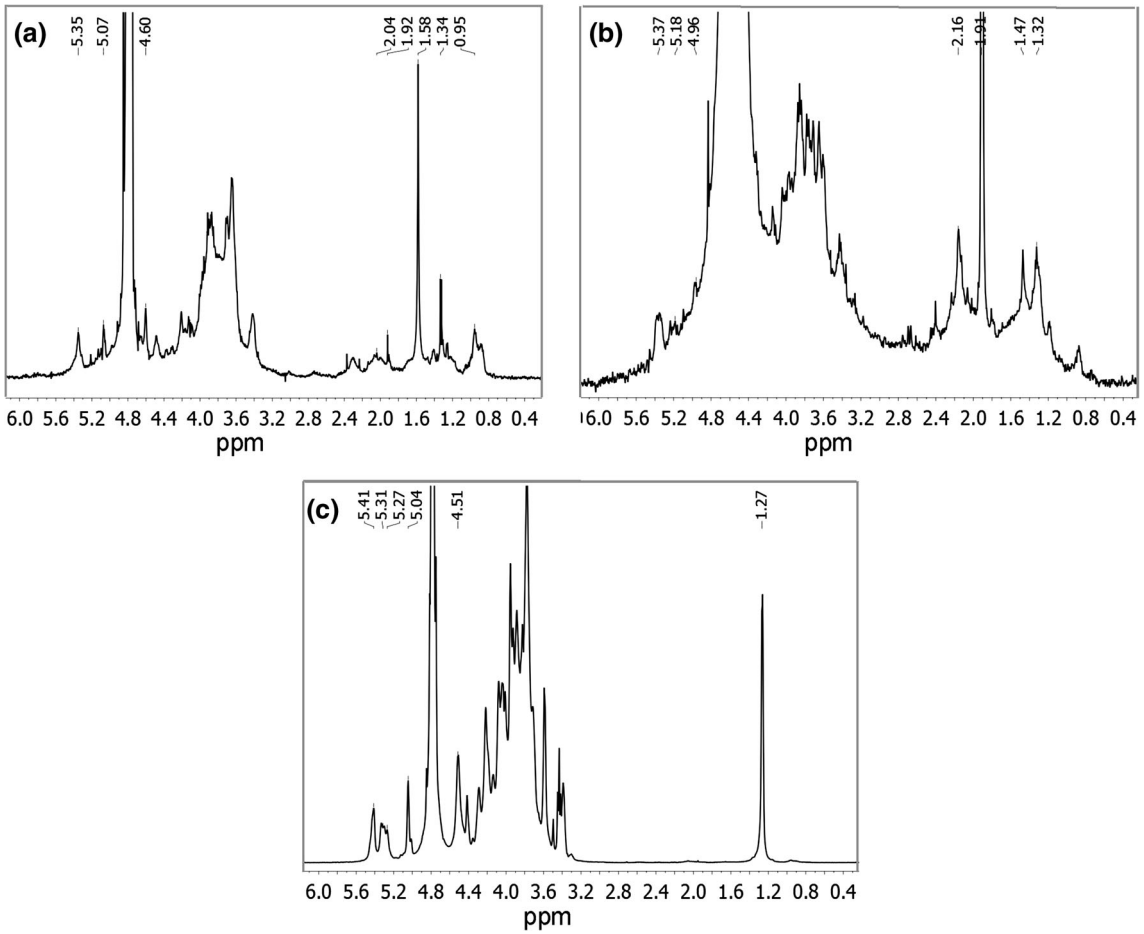

Fig. 4 ^{1}H NMR spectra of biopolymers, **a** microbactan at 25 °C, peaks at 4.6, 5.35 and 5.07 ppm, corresponds to hexose protons, **b** xanthan gum at 45 °C shows pyruvate at 1.47 and 1.32 ppm and acetate groups at 2.16 ppm, **c** arabic gum at 25 °C, peak at 1.27 ppm was assigned to methyl group of rhamnose

were only detected for microbactan and xanthan. These thin films had a slight roughness; however, they showed good adherence and seal to the superficial microporosity. On the other hand, arabic gum polymer had an opposite behavior, since no surface differences were observed between the two rocks under the microscope after the application of the coating (Fig. 5c, and ć).

In a previous work using photoacoustic technique, it was possible to study the permeability process of two types of limestones with different effective porosities by following the evolution of the thermal dynamics during the water diffusion process. Those studies allowed determining water diffusion coefficients, which could be associated directly with the interconnected porosity of the stones. The D values range was 20–330 $\times$ 10^{-6} cm^2 s^{-1} for two types of limestone [16]. In the present work, using a similar experimental configuration, the influence of a polysaccharide on the stone permeability is evaluated.

The characteristic curve obtained by PAS represents the typical behavior of a permeability process for non-treated rocks and rocks coated with the polymeric films (Fig. 6). The process showed three stages: the first stage corresponds to the situation before the water drop was deposited on the rock surface. The most important behavior is the second stage, because the signal is directly related to the permeability process and depends on the effective porosity of the substratum. Finally, the third stage is related to the stabilization of the process [16].

In general, all samples had different decay times. Additionally, they also showed a different decrease in the amplitude. The curves of RP (high porosity) exhibited a stronger decrease in the amplitude; therefore, the decay time was shorter in comparison with RL (low porosity), because RP stones had a higher effective porosity, and thus, the permeability process was faster. This behavior was more marked for the non-treated (control) and arabic gum-coated substrata (lithotypes), because the surface porosity remained unchanged, as it has been seen by SEM (Fig. 5c, and ć). This means that the surface porosity was not affected by the arabic gum coating. In contrast, the

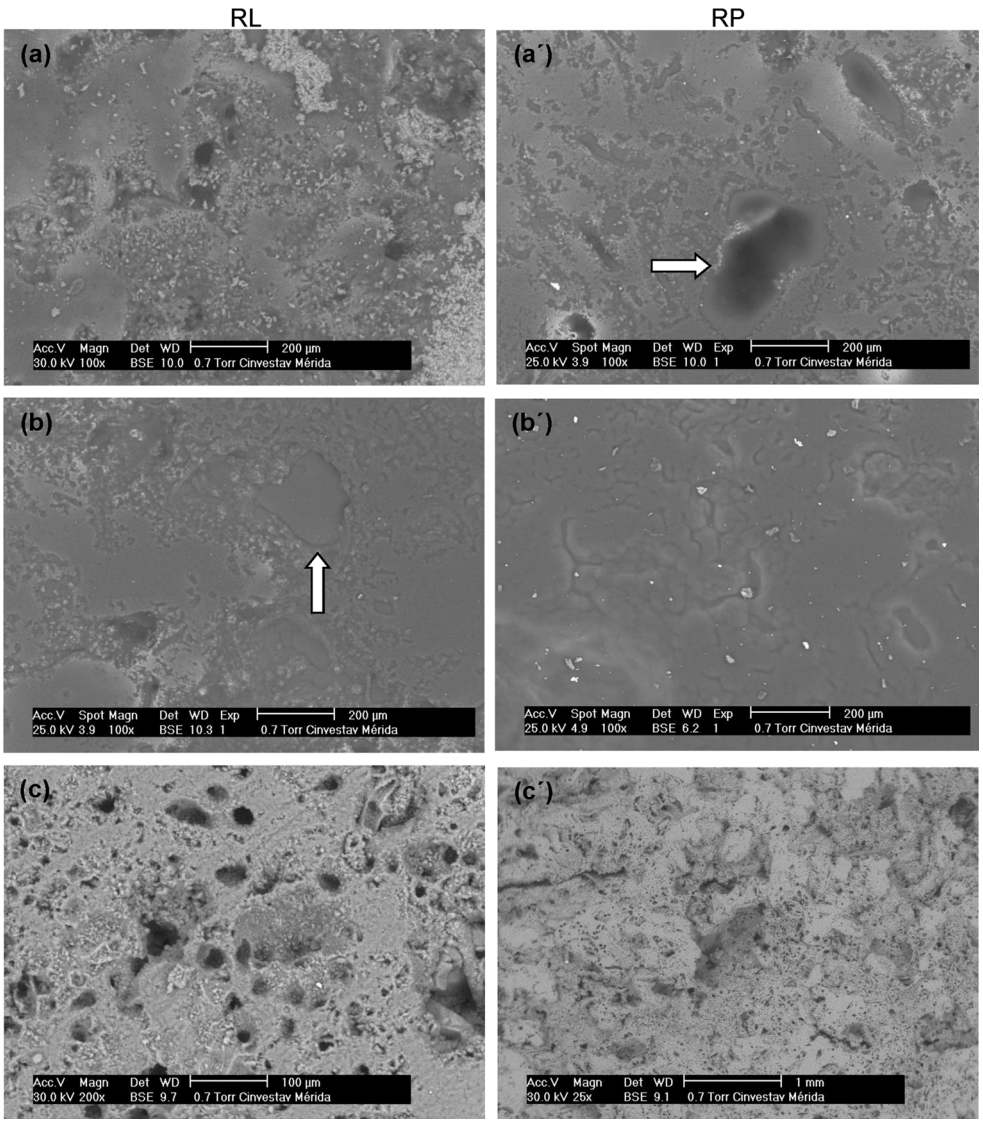

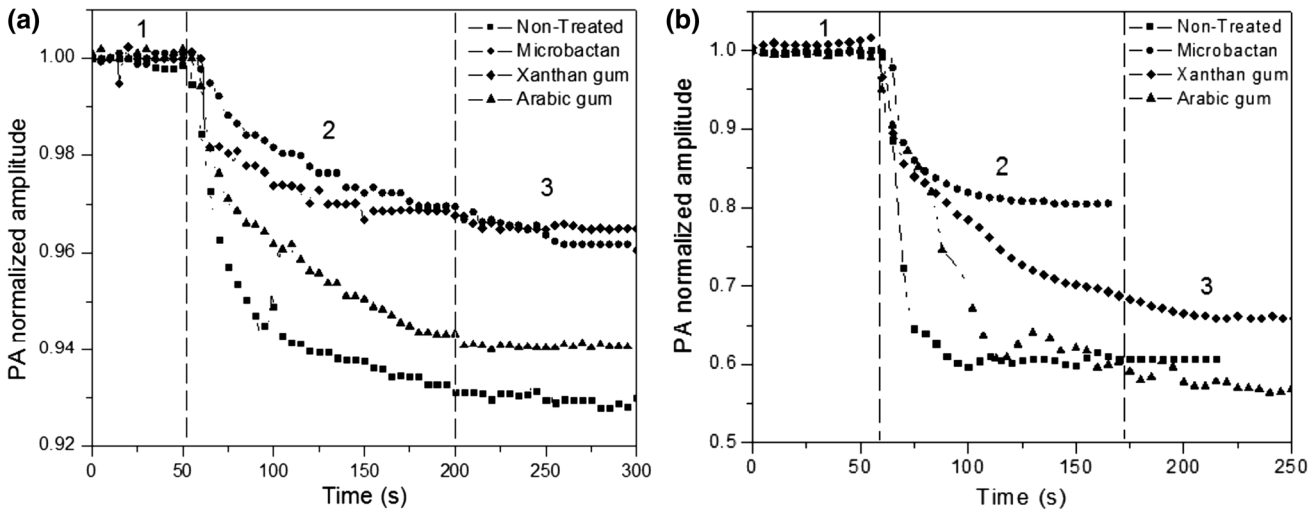

Fig. 5 SEM images collected on the rock surfaces with polymeric films. For RL, **a** microbactan, **b** xanthan gum, *arrow* indicating biopolymer coating in surface and **c** arabic gum, and for RP, **á** *arrow* showing coating microbactan biopolymer on the limestone surface, **b́** xanthan, and **ć** arabic gum

Fig. 6 Photoacoustic signal amplitude as a function of time during the permeability process for the non-treated and coating polymeric film rock: **a** RL and **b** RP

Table 2 Water diffusion coefficient values

Treatment	RL (low porosity)	RP (high porosity)
Water diffusion coefficient (D)		
Uncoated	$90 \pm 7 \times 10^{-6}$ cm^2 s^{-1}	$630 \pm 37 \times 10^{-6}$ cm^2 s^{-1}
Arabic gum coating	$76 \pm 9 \times 10^{-6}$ cm^2 s^{-1}	$423 \pm 25 \times 10^{-6}$ cm^2 s^{-1}
Microbactan coating	$49 \pm 5 \times 10^{-6}$ cm^2 s^{-1}	$160 \pm 14 \times 10^{-6}$ cm^2 s^{-1}
Xanthan gum coating	$50 \pm 8 \times 10^{-6}$ cm^2 s^{-1}	$110 \pm 30 \times 10^{-6}$ cm^2 s^{-1}

microporosity is sealed when microbactan and xanthan coatings were applied, which partially prevented the entry of water into the substratum, and therefore acted as a biobarrier. As a consequence, the permeability process was slower, as the water slowly flowed through the few interconnected pores or through the flow channels in a most heterogeneous system.

From the obtained curves (Fig. 6), it is possible to obtain the water diffusion coefficient from the fitted experimental data [16]. Table 2 shows the water diffusion coefficient values based on the two types of rock samples (RL and RP) with three different biopolymer coatings and the control (uncoated). Both controls (RL and RP, uncoated) presented the highest values of water diffusion coefficient, being the highest value in RP. Thus, it was observed that in RP the water was transported seven times faster, which was expected due to the surface porosity of the rock. Likewise, important differences of D values were observed both for controls and for biopolymers, the highest being values for RP. For example, the water diffusion coefficient was seven times higher in RP coated with arabic gum than that observed in RL. Microbactan and xanthan gum-coated surfaces showed a similar magnitude presenting the lowest values of water diffusion coefficient. These results indicate that the water transport is dependent on the chemical nature of the tested biopolymer and the substratum surface porosity. Even though there is no evident change in the porosity due to the arabic gum treatment when using microscopy observations, the sensitiveness of the PA technique can be seen in the differences in the water diffusion coefficient for the treated and untreated samples.

4 Discussion

Moisture controls to a great extent the chemical and physical processes that lead to stone decay. Biopolymers associated with microbial biofilms may either enhance or inhibit these processes, depending on a number of factors including polymer chemistry. However, there is limited understanding of the water transport across rocks under the influence of biopolymers. In this study, we hypothesized that the presence of coating biopolymers on the surfaces of rocks diminishes the diffusion coefficient, slowing down the transport of water across the rock sample. For this purpose, we used photoacoustic spectroscopy, which revealed as a useful tool to monitor the transport of water in real time on two types of limestone rocks of similar mineralogy but contrasting porosity under the influence of three biopolymers of varying chemistry. The results obtained in the course of this study confirmed our working hypothesis.

Our results have different implications for rock stability and conservation. On the one hand, the application of polymeric materials is a widely accepted strategy to minimize the effects of water penetration into the rock; most recently, a variety of synthetic polymers have been studied and developed as protecting agents for stone substratum [24]. Polymeric consolidants, including acrylics, silicones, vinyls, polyesters, urethanes and epoxies, aim to strengthen the stone by introducing macromolecules that solidify when the solvent evaporates or when curing agents cross-link with the resin, hence creating a solid network that can bond the grains together [25]. However, the use of biopolymers as consolidants or water repellent may lead to several problems, mainly related to the penetration depth, yellowing by ultraviolet rays, and biodeterioration owing to bacterial and fungal growth [25–27]. On the other hand, the changes in water transport in biopolymer-coated surfaces (considering biopolymers as a basic proxy for biofilm colonization) suggest that biofilm may retard water intake into the stone, slowing down deterioration processes.

Recently, several methods based on the induction of biogenic calcite into the pores of limestone have been developed. A relevant conservation treatment consists in using bacterially induced mineralization, which induces extracellular precipitation of calcium carbonate on decayed stone [11, 28]. In this case, the biomineralization process can occur by two mechanisms, biologically controlled or induced. In the first case, the organism controls the process; in the second, the cellular activity is what directs the formation, growth, and morphology of the minerals. Emerging evidence now suggests that EPS inhibit, alter or enhance precipitation of calcium carbonate [11]. Furthermore, EPS-mediated carbonate production may have a relevant role in the biology of biofilms. Interestingly, a recent study suggested that extracellular calcite scaffolds of biofilms may diminish the water transport within EPS matrix, which, in

turn, has consequences to eradicate biofilms (penetration of biocides) or to induce biomineralization [8].

Although RL and RP have a very similar chemical composition, it was observed that the effective surface porosity of RP was higher (almost five times). FTIR results showed that microbactan and xanthan gum had similar chemical characteristics, in comparison with arabic gum. It is relevant to mention that the coatings showed a similar coverage for both polymers when applied onto the rock samples. The coatings exhibited good adherence (Fig. 5); thus, it was possible to obtain good results even at low concentrations 1% (w/v). This adherence may be related to a number of factors: first, the presence of anionic substituents (acetate and pyruvate) and of negatively charged glucuronic, galacturonic, or mannuronic acids, known to participate in calcium complexation and second, given that these polymers have high molecular weight (typical molecular size of biopolymers in EPS range from 10^3 to 10^8 kDa [10].

The chemical and physical properties of the rocks are very different, having important consequences on rocks resistance toward weathering. As it was mentioned before, the decay of stone materials is a consequence of their interaction with the environment. In particular, transport of water is fundamental in the stone deterioration phenomena [29]. Decay processes of stone materials are related to physical, chemical and biological phenomena occurring mainly in the presence of water [24, 30]. The transport of water is one of the most important factors determining their durability in building construction stones and historical monuments, as it favors weathering processes such as acid dissolution in calcareous materials, growth of biological species, crystallization of soluble salts, and the swelling–contraction cycles due to hydration and temperature changes during day and night, in tropical environments [16]. The penetration of water through the surface (e.g., by capillary absorption) represents one of the main causes of stone degradation [24]. Water penetration is strongly affected by the open and effective porosity of stones and generally increases as a consequence of weathering [24, 31]. Weathering causes changes in the porosity because it can induce restructuring of pore size distribution, pore geometry, pore connectivity, pore infilling and formation of new pores [32]. The limestone materials analyzed in this work are highly porous and consequently can absorb large quantities of water (see Table 1). It is well known that the transport properties of rocks are conditioned by their permeability and porosity systems, since they control the movement and storage of fluids, being the permeability one of the properties which has a strong impact on rock weathering [16]. The network of EPS has a great capacity of water absorbance, being capable of binding more than 15–20 g of water per gram of EPS, and in the case of xanthan, 50–70 g of water can even be reached. Small amounts of EPS may significantly reduce the hydraulic conductivity in porous mediums; this was tested by Or et al. [10] who determined that the hydraulic conductivity is reduced from 10^{-5} to 10^{-6} ms^{-1} using a column of glass beads and a concentration of 1% (w/v) EPS.

In order to reduce these phenomena, the rate of water penetration into the rock should be reduced, for instance by means of a protective material [24]. Several materials and novel methodologies, able to protect these types of stones, have been developed. Consolidation is a strategy of conservation for building stones and architectural monuments, in an attempt to preserve the external weathered layers of stone and reduce their degradation rate [33]. However, some consolidation treatments are prone to cause undesired effects when applied to the stones [34]. Melo et al. [35] studied the photodegradation of acrylic resin films deposited onto dolomite rock. Those authors observed that polymers may present a yellowish color change, followed by discoloration, and in such experiments, the total elimination of the coating was possible.

Therefore, the biomineralization process induced by the exopolymers can act as a natural biorestorer. For this reason, the use of EPS represents an alternative in the area of stone biorestoration. However, the effect of the EPS layers on the surface properties and transport in the stone is relatively unexplored.

5 Conclusions

The permeation process of calcareous stone with different porosities and its surface coated with different polymers was studied by photoacoustic spectroscopy. The xanthan and microbactan biopolymers deposited on the surface formed a thin polymeric film and presented a good adherence for both types of rock. This adherence was probably related, at least partially, to the chemistry of biopolymers, notably the presence of acetate and pyruvate. The water diffusion coefficients are directly related to the effective surface porosity; however, the presence of the polymeric film significantly diminishes the water diffusion coefficient values. The transport coefficient D had higher values for the non-treated (uncoated) stones and for those coated with arabic gum. In contrast, coatings of microbactan and xanthan film polymers showed a good interaction with the surface of the stone, partially sealing the microporosity. The implications for reduced water transport in stone stability and conservation under the influence of biopolymers include both enhanced deterioration by slowing down the drying process of stone interiors, keeping moist conditions for chemical and physical

damaging processes. On the other hand, biopolymers may limit incoming (rain) water from entering the interior sections of stones, diminishing water uptake and subsequent deterioration. Although preliminary, this study showed that biopolymeric coatings as a basic proxy of biofilms suggest the active role of EPS matrix in stone deterioration. Similarly, the treatment of stone with natural (biopolymers) may have deteriogenic activity and should be regarded with caution. Finally, it is tempting to speculate that damaging epilithic biofilms may prove difficult to eradicate with water-soluble biocide treatments, which would be of limited value due to low water diffusion coefficients across the EPS matrix.

Acknowledgements The authors want to express their acknowledgment to J. Bante-Guerra for his help in the cell and electronics construction, D. Aguilar-Treviño for his help in the X-ray analysis, Ana R. Cristobal-Ramos and W. Cauich for their invaluable help in obtaining SEM and optical images, respectively. J. May-Crespo was funded by a postdoctoral fellowship of the program "Estancias postdoctorales vinculadas al fortalecimiento de la calidad del posgrado nacional 2012 PNPC-CONACYT" granted to B. O. Ortega-Morales. This study was supported by CONACYT 49275-F (24214), 188345, 204822, LAB-2009-01-123913, FOMIX-Yucatán No. 108160 and 108528 projects.

References

1. H.A. Viles, Geol. Soc. Lond. Spec. Publ. **205**, 407 (2002)
2. H.A. Viles, N.A. Cultler, Glob. Change Biol. **18**, 2406 (2012)
3. B.J. Smith, S. McCabe, D. McAllister, C. Adamson, H.A. Viles, J.M. Curran, Environ. Earth Sci. **63**, 1691 (2011)
4. A. Shearer, B.O. Ortega-Morales, C. Gaylarde, Adv. Appl. Microbiol. **66**, 97 (2009)
5. H.C. Fleming, J. Wingender, Nat. Rev. Microbiol. **8**, 623 (2010)
6. J. Tourney, B.T. Ngwenya, Chem. Geol. **386**, 115 (2014)
7. B.O. Ortega-Morales, J. Narváez-Zapata, M. Reyes-Estebanez, P. Quintana, S.C. De la Rosa-García, H. Bullen, S. Gómez-Cornelio, M.J. Chan-Bacab, Front. Microbiol. **7**, 201 (2016)
8. Y. Oppenhaimer-Shaanan, O. Sibonny-Nevo, Z. Bloom-Ackermann, R. Suissa, N. Steinberg, E. Kartvelishvily, V. Brumfeld, I. Kolodkin-Gal, N. P. J. Biofilms Microbiomes **2**, 15030 (2016)
9. W. De Muynck, N. De Belie, W. Verstraete, Ecol. Eng. **36**, 118 (2010)
10. D. Or, S. Phutane, A. Dechesne, Vadose Zone J. **6**, 298 (2007)
11. A.W. Decho, Ecol. Eng. **36**, 137 (2010)
12. S. McCabe, P. Brimblecombe, B.J. Smith, D. McAllister, S. Srinivasan, P.M.A. Basheer, Geol. Soc. Lond. **46**, 469 (2013)
13. O. Sass, H. Viles, J. Cult. Herit. **7**, 257 (2006)
14. F. Cerdeira, M.E. Vázquez, J. Collazo, E. Granada, Ener. Build **43**, 1845 (2011)
15. L. Pel, H. Huinink, K. Kopimga, Appl. Phys. Lett. **81**, 2893 (2002)
16. J. May-Crespo, P. Martínez-Torres, J.J. Alvarado-Gil, P. Quintana, J. Ordóñez-Miranda, Int. J. Thermophys. **3**, 1027 (2010)
17. J.C. Camacho-Chab, J. Guézennec, M.J. Chan-Bacab, E. Ríos-Leal, C. Sinquin, R. Muñiz-Salazar, S. De la Rosa-García, M. Reyes-Estebanez, O. Ortega-Morales, Int. J. Mol. Sci. **14**, 18959 (2013)
18. ASTM D2216-98, *Standard test method for laboratory determination of water (moisture) content of soil and rock by mass* (ASTM International, West Conshohocken, 2007)
19. H. Yavuz, S. Demirdag, S. Caran, Int. J. Rock Mechan. Min. Sci. **47**, 94 (2010)
20. B.O. Ortega-Morales, J. Santiago, M.J. Chan-Bacab, X. Moppert, E. Miranda-Tello, M. Fardeau, J.C. Carrero, P. Bartolo-Pérez, A. Valadéz-González, J. Guezennec, J. Appl. Microbiol. **102**, 254 (2007)
21. L. Vilca-Quispe, J.J. Alvarado-Gil, P. Quintana, J. Ordonez-Miranda, Int. J. Thermophys. **31**, 987 (2010)
22. E. Hecht, *Optics*, 4th edn. (Pearson Education Inc., San Francisco, 2002)
23. C.G. Kumar, H.S. Joo, J.W. Choi, Y.M. Koo, C.S. Chang, Enzym. Microb. Tech. **37**, 673 (2004)
24. M. Licchelli, M. Malagodi, M.L. Weththimuni, C. Zanchi, Prog. Org. Coat. **76**, 495 (2013)
25. E. Sassoni, S. Naidu, G.W. Scherer, J. Cult. Herit. **12**, 346 (2011)
26. S. Grassi, M. Favaro, P. Tomasin, L. Dei, J. Cult. Herit. **10**, 347 (2009)
27. D. Pinna, B. Salvadori, M. Galeotti, Sci. Total Environ. **423**, 132 (2012)
28. C. Jimenez-Lopez, F. Jroundi, C. Pascolini, C. Rodriguez-Navarro, G. Piñar-Larrubia, M. Rodriguez-Gallego, M.T. Gonzalez-Muñoz, Int. Biodeterior. Biodegrad. **62**, 352 (2008)
29. K. Beck, O. Rozenbaum, M. Al-Mukhtar, A. Plançon, International symposium on the conservation of monuments in the Mediterranean basin (arXiv:physics/0609111) (2009)
30. Th Warscheid, J. Braams, Biodeterioration of stone: a review. Int. Biodeterior. Biodegrad. **46**, 343 (2000)
31. E. Franzoni, E. Sassoni, G.W. Scherer, S. Naidu, J. Cult. Herit. **14**, 85 (2013)
32. A. Tugrul, Eng. Geol. **75**, 215 (2004)
33. I. Karatasios, P. Theoulakis, A. Kalagri, A. Sapalidis, V. Kilikoglou, Constr. Build. Mater. **23**, 2803 (2009)
34. A.P. Ferreira Pinto, J. Delgado Rodrigues, J. Cult. Herit. **9**, 38 (2008)
35. M.J. Melo, S. Bracci, M. Camaiti, O. Chiantore, F. Piacenti, Polym. Degrad. Stab. **66**, 23 (1999)